



Surface properties and visible light activity of W-TiO₂ photocatalysts prepared by surface impregnation and sol–gel method

Ewelina Grabowska^{a,*}, Janusz W. Sobczak^b, Maria Gazda^c, Adriana Zaleska^a

^a Department of Chemical Technology, Gdansk University of Technology, 80-233 Gdansk, Poland

^b Laboratory of Electron Spectroscopies, Institute of Physical Chemistry Polish Academy of Sciences, 01-224 Warsaw, Poland

^c Department of Solid State Physics, Faculty of Applied Physics and Mathematics, Gdansk University of Technology, 80-233 Gdansk, Poland

ARTICLE INFO

Article history:

Received 23 November 2011

Received in revised form 31 January 2012

Accepted 1 February 2012

Available online 10 February 2012

Keywords:

W-TiO₂

Modified-TiO₂

Doped-TiO₂

Tungsten

Visible light photocatalysis

Heterogeneous photocatalysis

ABSTRACT

Preparation route of new tungsten-containing TiO₂ powders (W-TiO₂) and their activity under visible light are reported. The photocatalysts were prepared by the sol–gel method and by grinding anatase powder with a dopant precursor followed by calcinations (surface impregnation method). Tungsten oxide and tungsten hexacarbonyl were used as tungsten sources in both photocatalyst preparation procedure. The obtained photocatalysts were subsequently characterized by a BET method, X-ray photoelectron emission spectroscopy (XPS) and X-ray powder diffraction analysis (XRD). Degradation efficiency of phenol and formation of phenol degradation by-products were compared for two systems: W-doped TiO₂ under visible light and P-25 under UV irradiation. The highest photoactivity under visible light was observed for 3%-W-TiO₂ and it was three times higher than photoactivity of pure TiO₂. Phenol oxidation in the presence of W-TiO₂ and visible light leads to formation of hydroxyproduct (catechol) and phenol ring cleavage products (muconic aldehyde).

© 2012 Elsevier B.V. All rights reserved.

1. Introduction

TiO₂ powder is well known as one of the suitable semiconductors for a photocatalyst and has been widely applied in various photocatalytic fields, such as environmental purification, decomposition of organic contaminants and water photosplitting into H₂ and O₂ [1,2]. However, TiO₂ is a high energy band material (E_g=3.2 eV) that can only be excited by high energy UV irradiation with a wavelength no longer than 388 nm. Recently, various modifications have been performed on TiO₂ to extend its optical absorption edge into visible light region and to improve its photocatalytic activity, including nonmetal doping [3–6] sensitizing [7], metal deposition [8,9] and doping by transition metals or transition metal oxides [10,11].

One of the modifying metal oxides, which are widely used, is tungsten oxide WO₃, which can be used as an independent photocatalyst. Due to a multiplicity of possible types of light excitation, WO₃ has a broad range of band-gap values (E_g=2.6–3.3 eV) as reported in the literature [12–16]. The fundamental optical transition is of an indirect type with E_g=2.7–2.8 eV [16], thus ensuring considerable photocatalytic and photoelectrocatalytic activity for WO₃ even under visible light illumination [17]. Additionally, the formation of a monolayer of WO_x species on TiO₂ can significantly

increase surface acidity as WO₃ is 15 times more acidic than TiO₂ [18]. Because of the increased acidity WO₃/TiO₂ can absorb more hydroxyl groups and simultaneously more organic reactants on its surface. Tungsten oxide is also used in electrochromic windows, infrared switching devices and gas sensors for detecting NO₂, H₂S, NH₃, H₂, O₃ and H₂O [19].

Different preparation methods of TiO₂–WO₃ photocatalysts were applied, such as sol–gel [20], hydrothermal [21], impregnation [22] and ball milling [24]. High rate of phenol degradation in the presence of WO₃ using laser induced photocatalytic process was reported by Gondal et al. [25]. They found that a small value of the band gap (about 2.8 eV) improved efficiency of WO₃ in the photocatalytic reaction. Do et al. [22] found that the degradation rate of 1,4-dichlorobenzene was enhanced by addition of WO₃ on the surface of TiO₂. Li et al. [20] and Song et al. [26] prepared WO_x–TiO₂ photocatalysts by sol–gel and sol-mixing methods with different amounts of WO_x. The photocatalytic activity of the obtained powders was estimated by measuring the decomposition rate of methylene blue in aqueous solution under the visible light. They found that by doping WO₃ the degradation rate was enhanced under visible light. Li et al. [20] and Song et al. [26] proved that the optimum dosage of a tungsten dopant in TiO₂ was 3% and 1%, respectively. Shen et al. [27] synthesized W,N-co-doped TiO₂ by a two-step method, combined with the sol–gel and the mechanical alloying method. The photocatalytic activity of the obtained W,N-codoped TiO₂ powders, measured by photodiscoloration of methylene blue and photodegradation of sulfosalicylic acid, under

* Corresponding author. Tel.: +48 583472937; fax: +48 583472065.

E-mail address: egrab@chem.pg.gda.pl (E. Grabowska).

visible light irradiation were enhanced compared to Degussa P25 [27]. Lorret et al. [28] obtained nanocrystalline tungsten doped titanium dioxide powders by a sol–gel method based on hydrolysis of TiCl_4 in aqueous solution. Different tungsten precursors and contents were used for the photocatalysts preparation. Their effects as well as the effect of calcination temperature on photoactivity in the decomposition of methylene blue under ultraviolet (UVA) and visible light were investigated. It was proven that photoactivity of W-TiO₂ samples strongly depends on the tungsten content (maximum reached for a ratio between 1 and 2 mol%) and the precursor choice ($\text{WCl}_6 > (\text{NH}_4)_6\text{H}_2\text{W}_{12}\text{O}_{40} > \text{H}_2\text{WO}_4$) under UVA irradiation and increases with tungsten content under visible light. However, because of the fact that dyes have relatively large photoabsorption coefficients and their molecules can absorb photons, especially in the visible light region, photoreaction might be induced by visible light photoabsorption – dye sensitization – as well as by photoabsorption of the photocatalysts [29]. Ohtani [30] proved that photosensitive materials are not suitable as probe chemicals for photocatalytic activity tests, especially for the evaluation of activity under visible light. There are at least three reasons for their inappropriateness: the first one has been already mentioned – dyes absorb visible light; the second – the absolute molar amount of dye contained in the reaction system can be much smaller than that of a solid photocatalyst; and the last one – the mechanism of dye degradation is so complicated that the efficiency of the photocatalytic reaction cannot be measured [29].

In the present study W-TiO₂ samples were prepared by the sol–gel method and by surface impregnation method (grinding anatase powder with a dopant precursor followed by thermal treatment). Our objective was to determine how the photocatalytic degradation pathways in the presence of Vis/W-TiO₂ differ from that corresponding to the action of UV radiation in the presence of P-25 TiO₂. These comparisons are expected to provide some insight into the basic mechanism of the tungsten-doped TiO₂ and visible light assisted water treatment. Therefore, these measurements are considered to give more important information to understand the role of doped-metal ions in enhancement of visible light-driven photocatalytic activity. The photocatalytic activity was studied by photodegradation of phenol in the aqueous solution under visible light. The effect of tungsten content and preparation method on photocatalytic activity was systematically investigated. The degradation pathway was studied by identification of phenol degradation by-products, created after irradiation in the W-TiO₂/Vis system. The P-25/UV system was used as the reference. In the next part of our research hydroxyl radical formations was investigated. Indirect methods with selected trapping agents were used for •OH radical detection. Illumination of TiO₂ suspension containing methanol and O₂ lead to the formation of HCHO. Previous literature had indicated that methanol is commonly used as hydroxyl radical scavenger, since it does not react with photogenerated holes. According to our knowledge, phenol photodegradation pathway in the W-TiO₂/Vis system was investigated for the first time in this study.

2. Experimental

2.1. Materials and instruments

TiO₂ ST-01 powder having anatase crystal structure was obtained from Ishihara Sangyo, Japan (anatase, surface area 300 m²/g, particle size 7 nm). Titanium (IV) isopropoxide (97%) was obtained from Aldrich Chem. 99% tungsten oxide (WO₃) and 97% tungsten hexacarbonyl (W(CO)₆) from Sigma–Aldrich Co. was used as tungsten source in the preparation procedure without further purification.

Nitrogen adsorption–desorption isotherms were recorded at liquid nitrogen temperature (77 K) on a Micromeritics Gemini V (model 2365) and the specific surface areas were determined by the Brunauer–Emmett–Teller (BET) method. All samples were degassed at 200 °C prior to nitrogen adsorption measurements. BET surface area was determined by a multipoint BET method using the adsorption data in the relative pressure (P/P_0) range of 0.05–0.3.

The catalyst powder crystal structure was determined from XRD pattern measured in the range of $2\theta = 20\text{--}80^\circ$ using X-ray diffractometer (Xpert PRO-MPD, Philips) with Cu target ($\lambda = 1.542 \text{ \AA}$). The XRD estimation of the crystallite size was based on the Scherrer formula:

$$d = \frac{0.9\lambda}{(B_e - B_i) \cdot \cos \theta},$$

where λ is the X-ray wavelength, B_e indicates the measured breadth of a peak profile, while B_i is the ideal, non-broadened breadth of a peak and θ is the diffraction angle [31]. The value of B_i was estimated on the basis of the measurements performed for the standard sample of polycrystalline Si with large crystalline grains. The accuracy of the grain size analysis has been estimated to be about 20%.

X-ray photoelectron spectroscopy (XPS) experiments were performed in a PHI 5000 VersaProbe – Scanning ESCA Microprobe (ULVAC-PHI, Japan/USA) instrument at the base pressure below 5×10^{-9} mbar. Monochromatic AlK_{α} radiation was used and X-ray beam, focused to a diameter of 100 micrometer, was scanned on a 250×250 micrometer surface, at an operating power of 25 W (15 kV). Photoelectron survey spectra were acquired using a hemispherical analyzer at pass energy 117.4 eV with a 0.4 eV energy step, core-level spectra were acquired at pass energy 23.5 eV with a 0.1 eV energy step. All spectra were acquired with 90° between X-ray source and analyzer and with the use of low energy electrons and low energy argon ions for charge neutralization. After subtraction of the Shirley-type background, the core-level spectra were decomposed into their components with mixed Gaussian–Lorentzian (30:70) shape lines using the CasaXPS software and sensitivity factors supplied by PHI. The main Ti 2p_{3/2} peak for TiO₂ with binding energy BE = 458.60 eV was used as reference of binding energy scale. All measurements were conducted with use a dual (low energy electron and low energy argon ion) automatic charge compensation. However additional small charge shift correction was made by using as an internal standard the main component of the system, titanium dioxide. As a standard value of Ti 2p_{3/2} binding energy value of TiO₂, we selected the most common value in the NIST X-ray Photoelectron Spectroscopy (XPS) Database version 4, equal to 458.60 eV. Binding energy values of all peaks were adjusted accordingly to this value.

The diffuse reflectance spectra DRS were characterized using UV–Vis spectrometer (UVD 3500 Labomed, USA) equipped with an integrating sphere accessory for diffuse reflectance.

The morphology of hollow microspheres was observed by Scanning Electron Microscopy (SEM, LEO Electron Microscopy Ltd, England, 1430VP). The images were acquired at wide range of magnification (40,000–800,000) in normal, high resolution and ultra high resolution modes using 3.5 mm working distance, 200 V to 300 kV accelerating voltage and 30 A emission current.

2.2. Preparation of W-TiO₂ photocatalysts

W-TiO₂ photocatalysts were prepared by the surface impregnation method and sol–gel method and labeled as W-TiO₂-G and W-TiO₂-H, respectively. Titanium dioxide ST-01 from Ishihara-Sangyo, Japan, was used in the surface impregnation procedure. W-TiO₂ powders were prepared by grinding 3 g of ST-01 in an agate mortar with an appropriate amount of dopant precursors.

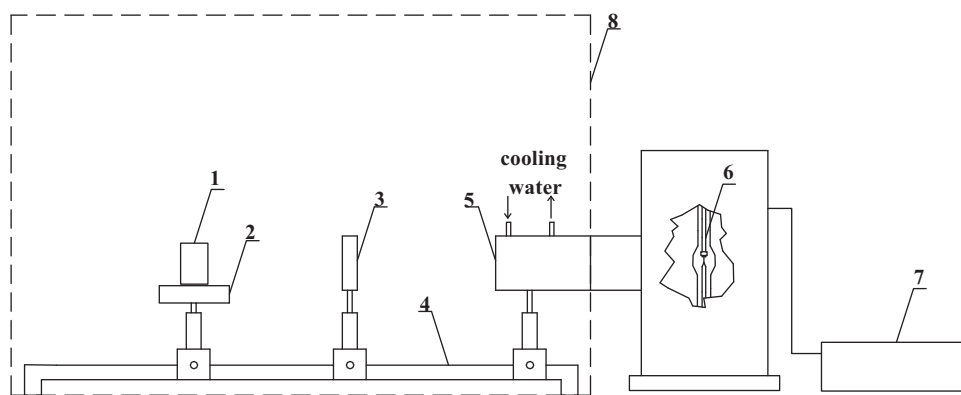


Fig. 1. Schematic diagram of the experimental set-up for examining the photocatalytic activity: 1 – cylindrical reactor with quartz window, 2 – magnetic stirrer, 3 – glass filter, 4 – optical bench, 5 – water filter, 6 – xenon lamp, 7 – power supply, 8 – black box.

The obtained powders were dried for 24 h at temperature 80 °C and calcinated at 400 °C or 450 °C for 1 h. In the sol–gel method, 10 ml titanium (IV) isopropoxide was mixed with an appropriate amount of the dopant precursor and 10 ml of distilled water. The solution was being stirred at room temperature for 45 min, followed by 24-h thermal treatment (80 °C) and calcinations at 400 °C for 1 h.

2.3. Photocatalytic activity test

The photocatalytic activity was estimated by measuring the decomposition rate of 0.21 mM phenol aqueous solution which was selected as a model contaminant. 25 ml of aqueous solution containing phenol was placed in a quartz photoreactor (i.d. 37 mm, length 30 mm) with 125 mg of TiO_2 photocatalyst. After 30 min aeration (5 dm^3/h) the suspension was irradiated with Xenon 1000 W lamp. The optical path included water filter and glass filters (GG) to cut off IR and UV irradiation. To limit the irradiation wavelength, the light beam was passed through GG400 filter to cut-off wavelengths shorter than 400 nm. The temperature during the experiments was maintained at 10 °C. One milliliter aliquots of the aqueous suspension were collected at regular time periods during irradiation and filtered through syringe filters ($\varnothing = 0.2 \mu\text{m}$) to remove photocatalyst particles. Phenol concentration was estimated by the colorimetric method ($\lambda = 480 \text{ nm}$) after derivatisation with diazo-p-nitroaniline using UV–Vis spectrophotometer (DU-7, Beckman).

A schematic diagram of the experimental set-up for the photocatalyst activity testing is presented in Fig. 1.

By-products formed during phenol degradation were identified by high performance liquid chromatography (HPLC) (Agilent 1200 system) attached to diode-array detector (DAD) and mass spectrometer (MS). A single quadrupole mass spectrometer with atmospheric pressure ionization was used. The initial concentration of phenol for intermediate product identification study was 1 mM. Higher initial concentration of phenol increased possibilities of isolation and identification of by-products. The P-25/UV system was chosen as the reference.

3. Results and discussion

3.1. Absorption properties

The amount of tungsten oxide and tungsten hexacarbonyl taken for photocatalysts preparation was calculated on the assumption that the content of tungsten in the sample after synthesis should be equal to 0.5–5 wt.% of the dry mass. All the photocatalysts obtained by grinding and by the sol–gel method followed by calcinations at 400 °C were in the form of beige powders. Sample labeling, the

kind and the amount of the dopant used during the preparation procedure and calcination temperature are given in Table 1.

Fig. 2 shows absorption spectra of W-doped TiO_2 prepared by grinding ST-01 with tungsten hexacarbonyl and tungsten oxide followed by calcination (Fig. 2A) and obtained by hydrolysis of TIP in the presence of tungsten precursor ($\text{W}(\text{CO})_6$) followed by thermal treatment (Fig. 2B). It is seen from Fig. 2 that almost all W-doped TiO_2 samples obtained by surface impregnation ST-01 with tungsten hexacarbonyl shows stronger absorption in the visible region than pure titanium dioxide. The lowest absorption was observed for W(3).G sample doped 3 wt.% of with tungsten oxide. A better optical absorption in the region of 400–700 nm is related to the presence of tungsten oxides. However, no correlation between absorption abilities and dopant content was observed. The best photoabsorption in the visible region was observed for WO(3).G sample obtained by grinding ST-01 with 3 wt.% of tungsten hexacarbonyl and for WO(1).H sample obtained by the sol–gel method using 1 wt.% of tungsten hexacarbonyl during the preparation. Our results are in good agreement with literature reports. Shen et al. [27] reported tungsten and nitrogen co-doped TiO_2 nanopowders with strong visible light response. The amount of W added varied from 0.5 to 10 wt.%. They found that samples prepared by adding 3 wt.% of tungsten possessed the best absorption ability in the visible light region. The group observed a correlation between photoabsorption and photoactivity. In the experiment of the photodiscoloration of MB sample containing 3 wt.% of tungsten revealed best photoactivity.

3.2. Crystal structure and BET surface area

XRD was used to investigate the phase composition and crystal structure of the as-prepared TiO_2 powders. The phase structure, crystallite size, crystallinity of TiO_2 and specific surface areas play important roles in photocatalytic activity and anatase phase of titania shows higher photocatalytic activity than brookite or rutile phase. XRD patterns of pure WO_3 and tungsten-modified TiO_2 prepared by impregnation and sol–gel method are shown in Figs. 3 and 4, respectively.

For all samples, no other phases were detected except anatase. No reflections corresponding to the formation of mixed oxides of $\text{TiO}_2\text{--WO}_3$ or pure WO_3 were seen in XRD patterns. The lack of reflections corresponding to WO_3 reveals that it is present either in the form of highly dispersed WO_x clusters or as an amorphous layer on TiO_2 as reported by several authors or the concentration of WO_3 is too low for the XRD to reveal. It was reported by Cordischi et al. [32] that only after annealing at temperatures as high as 1000 °C, the segregation of crystalline tungsten oxide can be observed by conventional XRD. Song et al. [26] concluded that W^{n+}

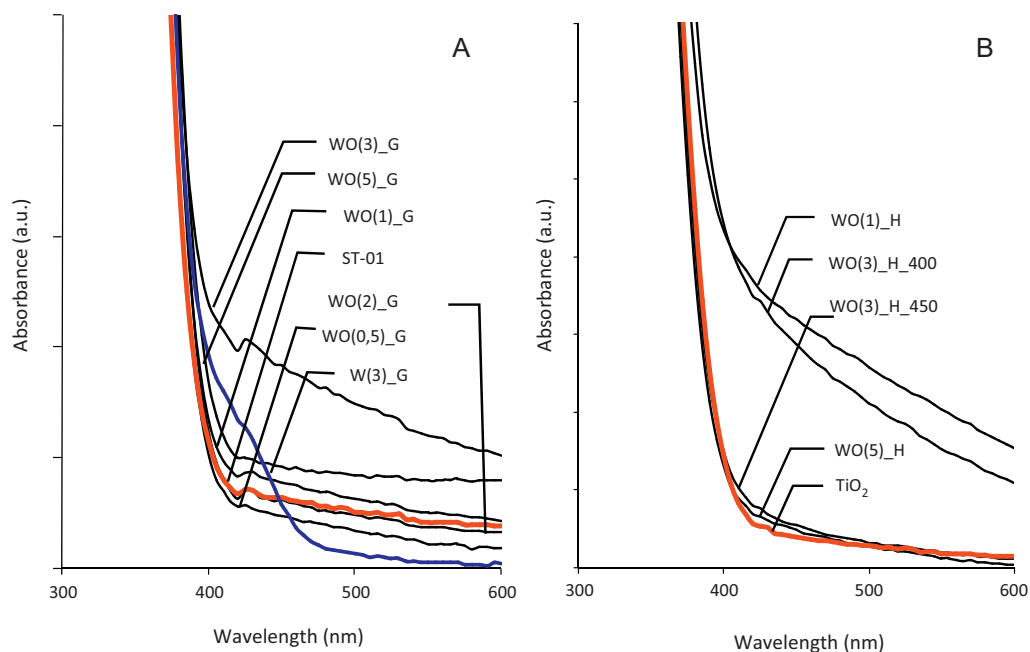


Fig. 2. UV-Vis/DR spectra of pure and W-doped TiO₂ prepared by (A) impregnation method (B) sol-gel method.

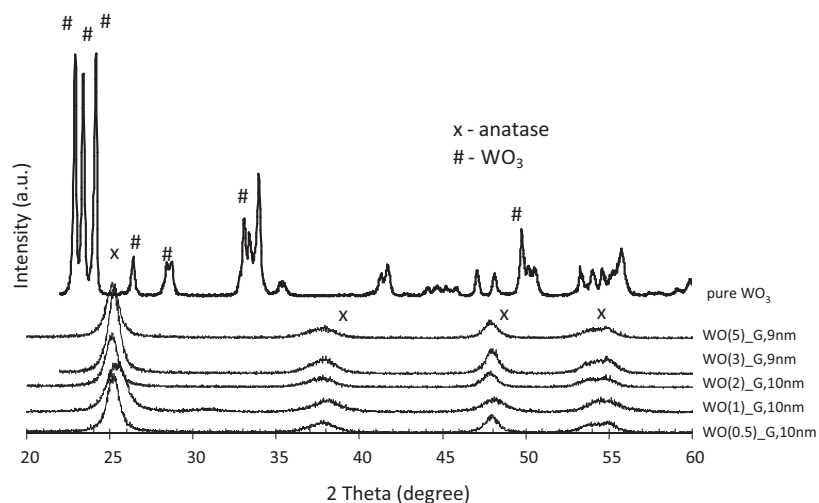


Fig. 3. XRD pattern of W-TiO₂ photocatalysts prepared by grinding TiO₂ ST-01 with a dopant.

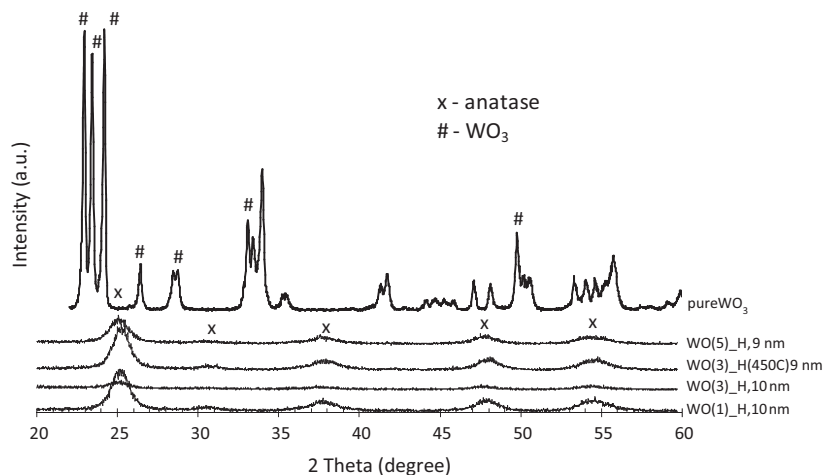


Fig. 4. XRD pattern of W-TiO₂ photocatalysts prepared by sol-gel method.

Table 1Characteristics of W-TiO₂ photocatalysts synthesized by sol–gel and grinding in the presence of tungsten oxide and tungsten hexacarbonyl.

Sample no.	Type of preparation method	Tungsten dopant	TiO ₂ precursor	Calcination temperature [°C]	Assumed content of tungsten [wt.%]
WO(1).H	Hydrolysis	W(CO) ₆	TIP	400	1
WO(3).H		W(CO) ₆	TIP	400	3
WO(3).H(450 °C)		W(CO) ₆	TIP	450	3
WO(5).H		W(CO) ₆	TIP	400	5
W(3).G		WO ₃	ST-01	400	3
WO(0.5).G	Surface impregnation	W(CO) ₆	ST-01	400	0.5
WO(1).G		W(CO) ₆	ST-01	400	1
WO(2).G		W(CO) ₆	ST-01	400	2
WO(3).G		W(CO) ₆	ST-01	400	3
WO(5).G		W(CO) ₆	ST-01	400	5

($4 < n < 6$) could substitute Ti(IV) in the lattice of TiO₂ because of the similarity in ion radius of Wⁿ⁺ (0.62–0.70 Å) and Ti(IV) (0.68 Å) to form non-stoichiometric solid solution of W_xTi_{1-x}O₂ that could produce tungsten impurity energy level. Furthermore Leghari et al. [33] suggested that all the tungsten ions may be incorporated into the titania lattice and replaced titanium ions to form W–O–Ti bonds or located at interstitial sites. A few authors reported that the addition of tungsten increases thermal stability of TiO₂ and stabilizes the anatase phase [34,35]. It was observed, that the addition of WO₃ did not induce any significant change in the phase composition.

In our data the average particles' size, determined on the base of Scherrer equations, ranged from 9 to 10 nm for all W-TiO₂ samples. The BET surface areas for the W-TiO₂.H and W-TiO₂.G series were listed in Tables 2 and 3, respectively. For all samples prepared by the surface impregnation method BET surface area was lower than for pure ST-01 TiO₂ and ranged from 170 to 192 m²/g. For the samples modified by adding 0.5–3 wt.% of tungsten precursor, the surface area varied from 170 to 175 m²/g, but the rise of tungsten precursor up to 5 wt.% resulted in the increase of the surface up to 192 m²/g. For the samples obtained by the sol–gel method, the surface area increased from 179 to 194 m²/g since the amount of tungsten precursor added during the preparation increased from 1 to 3 wt.%. Thus, it is easy to determine that the increase of tungsten concentration resulted in the increase of the surface area. This indicates that tungsten doping can confine the crystal growth, which may be beneficial for the photoactivity of W-TiO₂. Our observations are in good agreement with others. Shen et al. [27] observed larger BET surface area for higher concentration of tungsten in the case of (W,N) co-doped TiO₂ obtained by sol–gel method.

Table 2Photocatalytic activity under visible light presented as phenol degradation rate for W-TiO₂ samples prepared by impregnation method.

Sample no.	Surface area [m ² /g]	Phenol degradation rate [μmol dm ⁻³ min ⁻¹]
WO(0.5).G	175	1.0
WO(1).G	174	0.9
WO(2).G	173	0.9
WO(3).G	170	1.9
WO(5).G	192	0.8
Pure ST-01	276	0.6

Table 3Photocatalytic activity under visible light presented as phenol degradation rate for W-TiO₂ prepared by sol–gel method.

Sample no.	Surface area [m ² /g]	Phenol degradation rate [μmol dm ⁻³ min ⁻¹]
WO(1).H	179	1.7
WO(3).H	180	2.1
WO(3).H(450 °C)	163	1.1
WO(5).H	194	1.5
Pure TiO ₂	182	0.7

3.3. Surface composition

To study the chemical states of the prepared samples, XPS spectra were measured and analyzed. Table 4 shows atomic composition and chemical characters of the elements incorporated in the surface layer of the selected W-TiO₂ samples. The presence of both dopants in the surface layers was confirmed. The Ti 2p spectrum could be resolved into two components at binding energies ~459 and ~458 eV and were identified with TiO₂ and Ti₂O₃, respectively. Intensities of the decomposed components suggested that Ti(IV) was the dominant surface state. From 98.3 to 100% of titanium atoms were in the form of Ti(IV). The highest content of the reduced form of Ti atoms (Ti(III)) was observed for the sample WO(3).H. The quantitative analysis of tungsten content was difficult due to overlapping of Ti 3p and W 4f peaks. Only for the sample W(3).G, containing the highest amount of tungsten in the surface layer (0.3 at.%), the W 4f peak was clearly identified and separated from Ti 3p peak as shown in Fig. 5. The W 4f peaks of the prepared samples located at about 36–35 eV. Thus, the tungsten amount was estimated on the base of W 4d region. The XPS analysis of W 4f indicated that there were two components after deconvolution, as seen in Fig. 6. That could be attributed to the presence of tungsten in the form W(V) (BE W 4f_{7/2} = 35.0 ± 0.4 eV) and W(VI) (BE W 4f_{7/2} = 36.0 ± 0.4 eV). According to the literature data, the center of W 4f peak locates at about 35 eV, which is attributed to the formation of W–O bond in tungsten trioxide [36]. It was mentioned, that the electron is transferred from the conduction band of TiO₂ to the lower-lying conduction band of WO₃ to reduce the W(VI) to W(V) and the Ti(III) are oxidized to Ti(IV) by losing the electron. So the Ti(III) species are oxidized to Ti(IV) [23,25].

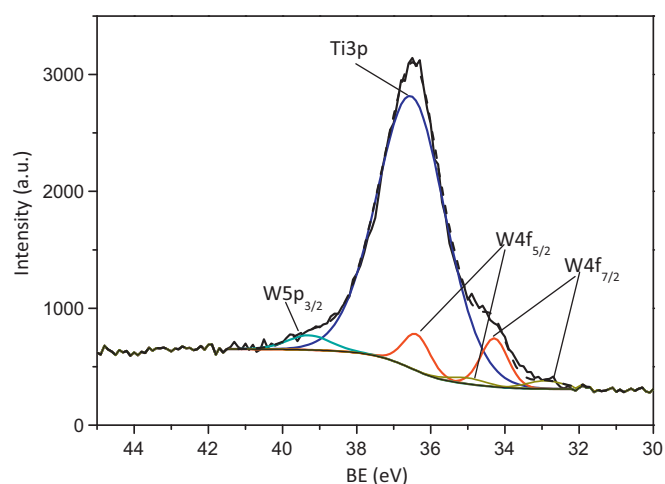
**Fig. 5.** XPS spectra of Ti 3p and W 4f region of the sample W(3).G.

Table 4
Atomic composition of TiO₂ samples doped with tungsten.

Sample label	Surface composition								Binding energy W 4f _{5/2} (eV)
	Σ Ti (at.%)	Ti(IV) 458.6 eV		Ti(III) 456.8 eV		Σ O (at.%)	Σ C (at.%)	Σ W (at.%)	
		(at.%)	(%)	(at.%)	(%)				
W(3).G	23.6	23.3	98.7	0.3	1.3	58.5	16.9	0.35	246.9
WO(3).G	23.8	23.5	98.9	0.3	1.1	58.4	17.0	0.15	247.1
WO(1).H	24.7	24.3	98.7	0.3	1.3	61.8	13.5	0.05	246.8
WO(3).H	21.8	21.4	98.3	0.4	1.7	60.1	18.1	0.01	248.4
WO(5).H	23.2	22.9	98.8	0.3	1.2	62.1	14.4	0.03	248.1

3.4. Photocatalytic decomposition of phenol

Photocatalytic activity of obtained TiO₂ powders was estimated by measuring the decomposition rate of phenol in aqueous solution in the presence of visible light irradiation ($\lambda > 400$ nm). No degradation of phenol was observed in the absence of photocatalyst or illumination. Pure TiO₂ synthesized by the sol–gel method without any dopant and ST-01 was used as the reference system. Photocatalytic activity under visible light is presented as phenol degradation rate (Tables 2 and 3) and as efficiency of phenol removal after 60 min of irradiation (Fig. 7).

Fig. 7A shows the results of phenol degradation under visible light in the presence of TiO₂ modified with tungsten hexacarbonyl synthesized by grinding TiO₂ powder with a dopant. Characteristic of photocatalysts is presented in Table 2. The highest photoactivity was observed for the sample prepared with 3 wt.% of tungsten hexacarbonyl. After 60 min irradiation of aqueous suspension initially containing 20 mg dm^{−3} of phenol, 47% of those was degraded. 27, 28, 24 and 21% of phenol was degraded in the presence of photocatalyst modified with 0.5; 1, 2 and 5 wt.% of tungsten hexacarbonyl, respectively.

Fig. 7B shows the influence of tungsten content on photocatalytic activity of powders prepared by the sol–gel method. Characteristic of photocatalysts is presented in Table 3. To study the effect of the calcination temperature sample W(3).H was calcinated in 400 and 450 °C. From all the samples containing different amounts of the dopant the highest photoactivity was observed for the sample prepared with 3 wt.% of tungsten hexacarbonyl calcinated at 400 °C. Phenol degradation rate was 2.1 $\mu\text{mol dm}^{-3} \text{ min}^{-1}$ for W(3).H sample, while for pure TiO₂ degradation rate equaled 0.7 $\mu\text{mol dm}^{-3} \text{ min}^{-1}$. After 60 min of irradiation 61% of phenol was degraded.

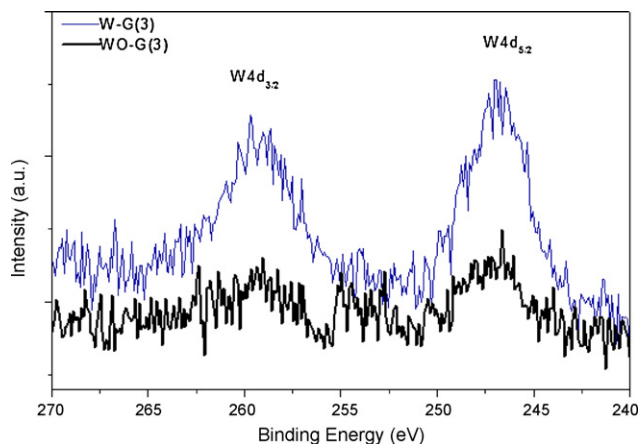


Fig. 6. XPS spectra of W 4d region of the samples W(3).G (prepared by grinding TiO₂ ST-01 with WO₃ followed by calcinations at 400 °C) and the sample WO(3).G (prepared by grinding TiO₂ ST-01 with W(CO)₆ followed by calcinations at 400 °C).

Experimental data clearly indicate the presence of correlation between absorption and photoactivity only for the powders obtained by surface impregnation method – for increased photoactivity absorption in visible region also increased. Sample WO(3).G

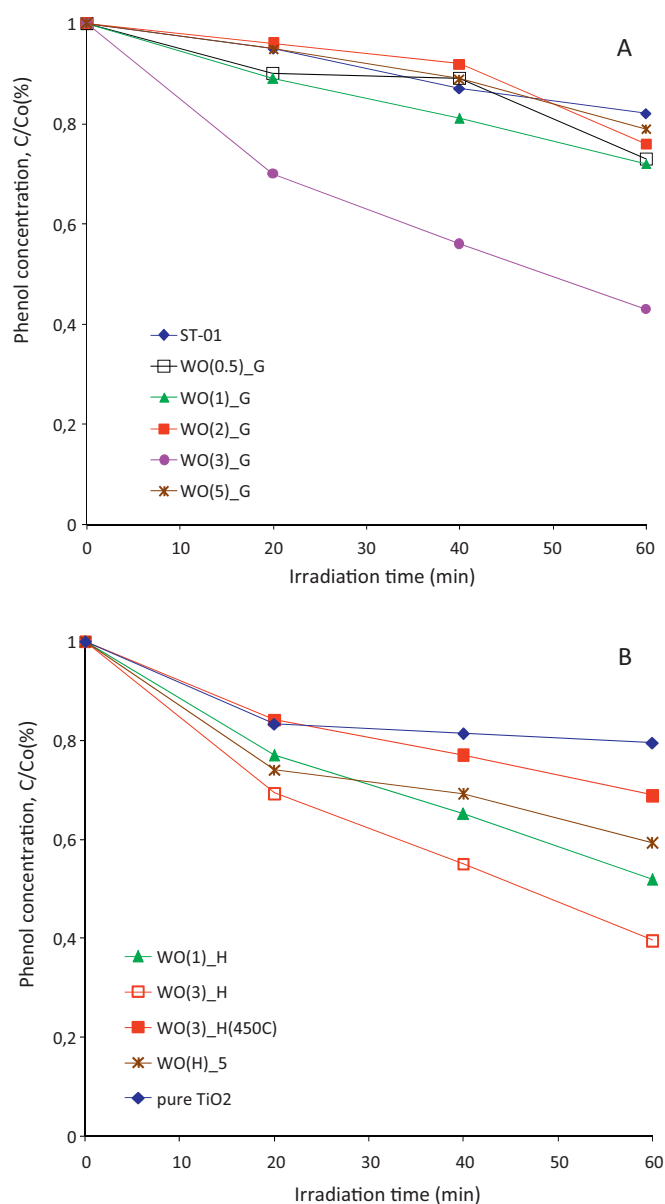


Fig. 7. Photoactivity under visible light of W-TiO₂ prepared by (A) surface impregnation method, (B) sol–gel method. Experimental conditions: $c_0 = 0.21$ mM; m (TiO₂) = 125 mg, $T = 10$ °C, $Q_{\text{air}} = 5$ l/h, $\lambda > 400$ nm.

– showing the highest photoactivity under visible light – revealed the best absorption in visible region.

Piszc et al. [38] prepared $\text{WO}_x\text{-TiO}_2$ photocatalysts by the sol–gel method from tetraisopropyl orthotitanate and WO_2 . The calculated amount of WO_x in TiO_2 was 3% wt. The obtained samples were calcined at 400–800 °C. The photoactivity was tested for phenol degradation in an aqueous solution under UV irradiation. The highest rate of phenol degradation was observed for $\text{WO}_x\text{-TiO}_2$ calcined at 500 °C. After 12 h of irradiation 25% of phenol was degraded [38]. Li et al. [20] observed 83.5% of TOC reduction (MB, $c_0 = 12.5 \text{ mg/l}$) for tungsten-doped TiO_2 prepared by a sol–gel method. $(\text{NH}_4)_{10}\text{H}_2\text{W}_{12}\text{O}_{42} \cdot 4\text{H}_2\text{O}$ was used as a tungsten source. The authors reported that the optimal content of WO_x in TiO_2 was found to be 3%, which is in good agreement with our results.

Lin et al. [39] prepared tungsten-doped TiO_2 samples to enhance 4-chlorophenol ($c_0 = 0.2 \text{ mM}$) rate and using the visible light energy source. The band gap edge wavelength increased to 475 nm. The results indicate that the removal of 4-CP up to 65% could be attained after 180 min of irradiation in the presence of TiO_2/WO_3 system (3% wt.).

Li et al. [40] prepared tungsten and nitrogen codoped TiO_2 nano-photocatalysts with twist-like helix structure with a facile and template-free one-pot method, which showed higher visible light response compared with pure TiO_2 and P25. The W,N- TiO_2 samples were synthesized by simple hydrolysis of titania tetrachloride using ammonium tungstate as tungsten and nitrogen source. The novel photocatalysts showed both high ultraviolet and visible light photocatalytic activity in degrading phenol, while the 1%-W,N- TiO_2 sample gave the best photocatalytic activity and demonstrated to be far superior to that of the commercial Degussa P25 counterpart. The higher photocatalytic activity of the 1%-W,N- TiO_2 sample is partially due to its high specific surface area, special helix structure and mesoporous pores, small crystallite size and good anatase crystallization. Moreover authors explain that when anatase TiO_2 is doped with tungsten species with changing valence, improved charge separation can result from doping the tungsten ions. The higher acidity of WO_3 than TiO_2 can modify the affinity of substrates for the catalyst surface and the adsorption equilibrium of the catalyst. When the addition value of WO_3 was higher than 1%, too much WO_3 deposited on the catalysts surface will act as trapping site by accepting the photo-excited electrons from the TiO_2 valence band, hence the photo-induced electrons and the photocatalytic activity decreased [40].

The band gaps of TiO_2 and WO_3 nanoclusters are all in the ultraviolet, and TiO_2 has a slightly larger band gap than WO_3 (band gaps of WO_3 and TiO_2 are 2.8 and 3.2 eV, respectively). TiO_2 can be excited by photons with wavelengths under 387 nm, which produces photo-generated electron–hole pairs and shows photocatalytic activity. Both the top of the valence band and the bottom of the conduction band of WO_3 are lower than those of TiO_2 . But when WO_3 and TiO_2 form a coupled photocatalyst, TiO_2 and WO_3 can be excited simultaneously under UV illumination. While studying coupled WO_3/TiO_2 systems, it has been found out [20,21] that the band-gap energy of the composite WO_3/TiO_2 is lower than that of WO_3 and the red shift in the absorption edge of the composite depends on the method of synthesizing, the nature of the precursors and on the temperature of calcinations of W- TiO_2 photocatalysts [37]. The recombination of photo-generated electrons and holes is one of the most significant factors that influence the photo activity of the samples. When WO_3 and titania form a composite photocatalyst, the photo excitation process occurs. The photogenerated holes can transfer from the WO_3 valence band to the TiO_2 valence band and the photogenerated electrons can transfer from the TiO_2 conduction band to the WO_3 conduction band [16,41]. Tungsten oxides added into TiO_2 could shift the light absorption

band from near UV range to the visible range and could hinder the recombination of the excited electrons/holes. The result is that the photogenerated carriers can be effectively separated and result in an improved coloration performance because W(VI) can be easily reduced to W(V). The result is that the WO_x/TiO_2 coupled photocatalyst exhibits higher photocatalytic activity than that of TiO_2 , which is in good agreement with the obtained results.

To summarize, the most visible-light active photocatalyst can be obtained by sol–gel method or by surface impregnation with 3 wt.% of tungsten hexacarbonyl used during the preparation route. The BET surface area of $\text{WO}(3)\text{G}$ and $\text{WO}(3)\text{.H}$ samples as well as photoactivity was quite close. Phenol degradation rate, in the presence of the $\text{WO}(3)\text{G}$ ($170 \text{ m}^2/\text{g}$) and the $\text{WO}(3)\text{.H}$ ($180 \text{ m}^2/\text{g}$) sample, equaled to 1.9 and $2.1 \mu\text{mol dm}^{-3} \text{ min}^{-1}$, respectively. Tungsten presence in the surface layer was confirmed for both samples by the XPS analysis. The surface analysis indicated that tungsten in the form of W(V) and W(VI) was successfully doped using both sol–gel and surface impregnation method. However, overlapping of Ti 3p and W 4f peaks impeded correlation between photoactivity and chemical composition of samples, due to unclear interpretation of chemical character of tungsten incorporated in the surface layer.

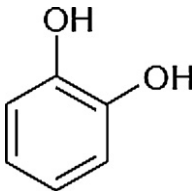
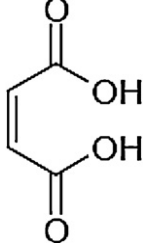
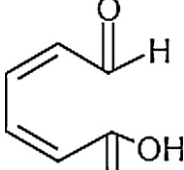
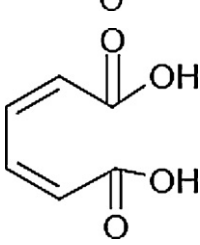
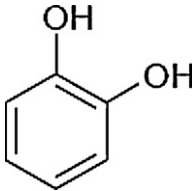
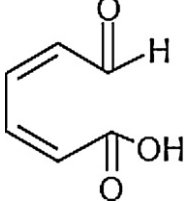
3.5. Phenol degradation pathway

Phenol degradation intermediates identified in the reaction mixture after 300 min irradiation in the Degussa P-25 TiO_2/UV , W- TiO_2/Vis systems are shown in Table 5. For Degussa P-25/UV system, catechol was detected as the main hydroxylation by-product. Moreover, muconic acid, muconic aldehyde and maleic acid were identified as the phenol ring cleavage products. Both, phenol hydroxylation products and aliphatic unsaturated acids are also reported by Górska et al. as phenol destruction intermediates formed during UV irradiation in the presence of pure and N,C-doped TiO_2 [42].

In the presence of tungsten modified TiO_2 and visible light only the presence of catechol and muconic aldehyde was confirmed using HPLC–MS. The presence of any of the unsaturated acids was not validated. Thus, the formation of the hydroxyproduct indicated activation of phenol molecule with $\bullet\text{OH}$ radical, in the presence of tungsten doped TiO_2 irradiated by visible light. It was contrary to our previous observation for non-metal-doped TiO_2 activated by visible light. It was found that in the presence of N,C- TiO_2/Vis none of phenol hydroxyproducts was present and hydroxybenzoic acid, oxalic acid and aldehyde were identified [42]. Oxalic acid is believed to be formed in one of the last steps of the photodegradation process due to breaking of the aromatic ring [42].

The presence of OH radical in W- TiO_2 system was additionally confirmed by methanol oxidation. The method consisted of $\alpha\text{-H}$ abstraction by hydroxyl radicals from methanol in aerated photocatalyst suspension, followed by determination of the principal stable product, formaldehyde [42]. The concentration of HCHO is proportional to $\bullet\text{OH}$ radicals concentration and the reaction efficiency is usually established at 70% [43]. The obtained results indicate that HCHO was created during exposition of W-doped TiO_2 to the visible light (see insert in Fig. 8). However, the yield of formaldehyde generation for W- TiO_2/Vis system was about hundred times less than for P-25 during UV–Vis irradiation. Formaldehyde concentration after 120 min. of methanol oxidation in the P25/UV–Vis and W- TiO_2/Vis system was 2.9 and 0.3 mM, respectively (see Fig. 8). Thus, the observed absence of another phenol degradation by-products in the W- TiO_2/Vis light system could be related to low efficiency of hydroxyl radical generation in this system. Comparing to P25/UV system,

Table 5
Phenol degradation intermediates identified after 300 min of irradiation in the presence of (a) P-25 Evonik and UV–Vis irradiation; (b) W-doped TiO₂ and Vis light. Experimental conditions: C_{phenol} = 1 mM, m (TiO₂) = 125 mg, T = 10 °C, Q_{air} = 5 l/h, UV–Vis light: λ > 250 nm, Vis light: λ > 400 nm.

Compound name	Molecular mass	Retention time (min)	Compound structure
P-25/UV–Vis			
Catechol	110	7.7	
Maleic acid	116	2.0	
Muconic aldehyde	125	11.4	
Muconic acid	142	2.8	
W-TiO ₂ /Vis			
Catechol	110	7.7	
Muconic aldehyde	125	11.4	

the amount of hydroxyl radicals was much lower and resulted amount of formed by-products could be too low to detect it using HPLC–MS.

Presented data indicated different degradation mechanism of phenol in the presence of tungsten-doped TiO₂ and visible light than in UV/TiO₂ system. The low concentration of OH• radicals suggested that phenol depletion resulted both from oxidation *via* OH radical as well as direct reaction with photogenerated carriers (e[−]/h⁺). This observation is in good agreement with others. The

increase in the single-electron transfer (SET) chemistry with the presence of WO_x was noted by Hathway et al. [44]. They examined the oxidative chemistry of two sets of photocatalysts: commercial PC50 and DT52 from Millenium coated with WO_x by an incipient wetness method and WO_x–TiO₂ photocatalysts prepared by sol–gel method. This might be explained either by greater adsorption of the organic to the modified photocatalysts or by longer lifetime of the SET-active “hole” before finding an alternative trap site that results in hydroxyl chemistry [44].

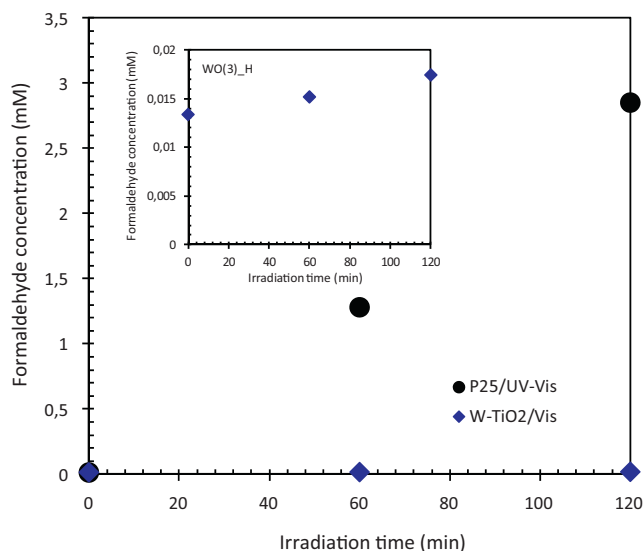


Fig. 8. Concentration of formaldehyde vs. irradiation time in the presence of P-25 and UV-Vis irradiation and W-TiO₂ and Vis irradiation. Experimental conditions: $C_{\text{methanol}} = 50 \text{ mM}$, $m(\text{TiO}_2) = 125 \text{ mg}$, $T = 10^\circ\text{C}$, $Q_{\text{air}} = 5 \text{ l/h}$, UV-Vis light: $\lambda > 250 \text{ nm}$, Vis light: $\lambda > 400 \text{ nm}$.

4. Conclusions

The effect of the preparation method on surface properties and photoactivity of W-TiO₂ was systematically investigated. The surface analysis indicated that tungsten in the form of W(V) and W(VI) was successfully doped using both sol-gel and surface impregnation method. The highest photoactivity was obtained when 3 wt.% of tungsten hexacarbonyl was introduced during titanium tetraiso-propoxide hydrolysis and the temperature at thermal treating step was 400°C . The obtained photocatalyst showed three times exceeded visible light photocatalytic activity than pure TiO₂. Thus, photodegradation in the presence of W-doped TiO₂ and visible light appears to be a promising process for pollutant degradation, utilizing solar energy. Using the 3% W-TiO₂ powder, the phenol degradation efficiency under visible light could reach 60% after 60 min treatment. Presented data suggested a different degradation mechanism of phenol in the presence of W-doped TiO₂ and visible light than in UV and pure TiO₂ system. Although the degradation of organic contaminants was efficient, very low efficiency of hydroxyl radical generation and in the W-doped TiO₂/Vis system was observed. However, phenol irradiation by visible light in the presence of suspended W-TiO₂ still leads to formation of hydroxy-product (catechol) and phenol ring cleavage products (muconic aldehyde).

Acknowledgements

This research was partially supported by the Voivodeship Fund for Environmental Protection and Water Management in Gdansk, grant no. WFOŚ/D/201/142/2009 and The Ministry of Science and Higher Education (contract no.: N523 568438)

References

- [1] A. Fujishima, X. Zhang, C.R. Chim. 9 (2006) 750–760.
- [2] M.R. Hoffmann, S.T. Martin, W. Choi, D.W. Bahnemann, Chem. Rev. 95 (1995) 69–96.
- [3] R. Asahi, T. Morikawa, T. Ohwaki, K. Aoki, Y. Taga, Science 293 (2001) 269–271.
- [4] A. Zaleska, J.W. Sobczak, E. Grabowska, J. Hupka, Appl. Catal. B 78 (2007) 92–100.
- [5] L. Gomathi Devi, K. Eraiah Rajashekhar, J. Mol. Catal. 334 (2011) 65–76.
- [6] W. Mekprasart, W. Pecharapa, Energy Procedia 9 (2011) 509–514.
- [7] P. Moro, M. Pia Donzello, C. Ercolani, F. Monacelli, G. Moretti, J. Photochem. Photobiol. 220 (2011) 77–83.
- [8] M. Maicu, M.C. Hidalgo, G. Colón, J.A. Navío, J. Photochem. Photobiol. 217 (2011) 275–283.
- [9] A. Zielińska-Jurek, E. Kowalska, J.W. Sobczak, W. Lisowski, B. Ohtani, A. Zaleska, Appl. Catal. B 101 (2011) 504–514.
- [10] U.G. Akpan, B.H. Hameed, Appl. Catal. A 375 (2010) 1–11.
- [11] S.K.S. Patela, N.S. Gajbhiye, S.K. Dateb, J. Alloys Compd. 509S (2011) S427–S430.
- [12] J. Georgieva, S. Armanov, E. Valova, I. Poulis, S. Sotiropoulos, Electrochem. Commun. 9 (2007) 365–370.
- [13] T. He, Y. Ma, Y. Cao, X. Hu, H. Liu, G. Zhang, W. Yang, J. Yao, J. Phys. Chem. B 106 (2002) 12670–12676.
- [14] M. Gillet, K. Aguir, C. Lemire, E. Gillet, K. Schierbaum, Thin Solid Films 467 (2004) 239–246.
- [15] I. Schiyanovskaya, M. Hepel, J. Electrochem. Soc. 146 (1999) 243–249.
- [16] M. Miyauchi, A. Nakajima, T. Watanabe, K. Hashimoto, Chem. Mater. 14 (2002) 4714–4720.
- [17] T. Ohno, F. Tanigawa, K. Fujihara, S. Izumi, M. Matsumura, J. Photochem. Photobiol. A 118 (1998) 41–44.
- [18] Y.T. Kwon, K.Y. Song, W.I. Lee, G.J. Choi, Y.R. Do, J. Catal. 191 (2000) 192–199.
- [19] X. Zhao, T.L.Y. Cheung, X. Zhang, D.H.L. Ng, J. Am. Ceram. Soc. 89 (2006) 2960–2963.
- [20] X.Z. Li, F.B. Li, C.L. Yang, W.K. Ge, J. Photochem. Photobiol. A 141 (2001) 209–217.
- [21] D. Ke, H. Liu, T. Peng, X. Liu, K. Dai, Mater. Lett. 62 (2008) 447–450.
- [22] Y. Do, W. Lee, K. Dwight, A. Wold, J. Solid State Chem. 108 (1994) 198–201.
- [23] K.Y. Song, M.K. Park, Y.T. Kwon, H.W. Lee, W.J. Chung, W.I. Lee, Chem. Mater. 13 (2001) 2349–2355.
- [24] C. Shifu, C. Lei, G. Shen, C. Gengyu, Powder Technol. 160 (2005) 198–202.
- [25] M.A. Gondal, M.N. Sayeed, A. Alarfaj, Chem. Phys. Lett. 445 (2007) 325–330.
- [26] H. Song, H. Jiang, X. Liu, G. Meng, J. Photochem. Photobiol. A 181 (2006) 421–428.
- [27] Y. Shen, T. Xiong, T. Li, K. Yang, Appl. Catal. B 83 (2008) 177–185.
- [28] O. Lorret, D. Francova, G. Waldner, N. Stelzer, Appl. Catal. B 91 (2009) 39–46.
- [29] X. Yan, T. Ohno, K. Nishijima, R. Abe, B. Ohtani, Chem. Phys. Lett. 429 (2006) 606–610.
- [30] B. Ohtani, Chem. Lett. 37 (2008) 216–229.
- [31] V. Uvarov, I. Popov, Mater. Charact. 58 (2007) 883–891.
- [32] D. Cordischi, D. Gazzoli, M. Occhiuzzi, M. Valigi, J. Solid State Chem. 152 (2000) 412–420.
- [33] S.A.K. Leghari, S. Sajjad, F. Chen, J. Zhang, Chem. Eng. J. 166 (2011) 906–915.
- [34] H. Yang, D. Zhang, L. Wang, Mater. Lett. 57 (2002) 674–678.
- [35] G. Ramis, G. Busca, C. Cristiani, L. Liotti, P. Forzatti, F. Breganis, Langmuir 8 (1992) 1744–1749.
- [36] J.F. Moulder, W.F. Stickle, P.E. Sobol, K.D. Bomben, Handbook of X-ray Photoelectron Spectroscopy, Publ. by ULVAC-PHI, Inc. Chigasaki, Japan, 1995.
- [37] G.R. Bamwenda, H. Arakawa, Appl. Catal. A 210 (2001) 181–191.
- [38] M. Piszcz, B. Tryba, B. Grzmil, A.W. Morawski, Catal. Lett. 128 (2009) 190–196.
- [39] C.F. Lin, C.H. Wu, Z.N. Onn, J. Hazard. Mater. 154 (2008) 1033–1039.
- [40] J. Li, J. Xu, W.-L. Dai, H. Li, K. Fan, Appl. Catal. B 82 (2008) 233–243.
- [41] D. Robert, Catal. Today 122 (2007) 20–26.
- [42] P. Górski, A. Zaleska, J. Hupka, Sep. Purif. Technol. 68 (2009) 90–96.
- [43] C. Wang, D.W. Bahnemann, J.K. Dohrmann, Water Sci. Technol. 44 (5) (2000) 279–286.
- [44] T. Hathway, E.M. Rockafellow, Y.C. Oh, W.S. Jenks, J. Photochem. Photobiol. A 207 (2009) 197–203.